

# MICROWELL-ARRAY ON A FLEXIBLE NEEDLE: A TRANSCUTANEOUS INSERTABLE IMPEDANCE SENSOR FOR LABEL-FREE CYTOKINE DETECTION

Naixin Song<sup>1</sup>, Pengfei Xie<sup>2</sup>, Wen Shen<sup>1</sup>, Mehdi Javanmard<sup>2</sup> and Mark G. Allen<sup>1</sup>

<sup>1</sup>School of Engineering and Applied Science, University of Pennsylvania, PA, USA

<sup>2</sup>School of Engineering, Rutgers University, NJ, USA

## ABSTRACT

Measurement of various specific proteins in body fluids can be a key component of continuous health monitoring. The gold-standard technique for protein quantification is ELISA, which typically relies on labeling and optical fluorescence. Impedance sensors provide a promising alternative due to ease of miniaturization, rapid readout and label-free operation; yet lag their fluorescent counterparts in terms of sensitivity. We present a flexible micromachined needle-shaped impedance sensor for label-free in-situ detection of cytokines and other biomarkers. The sensor utilizes a micro-well array configuration at the needle tip to enable label-free detection while simultaneously maintaining the capability of high sensitivity detection, despite the high salt concentration of complex biological fluids. Real-time label-free detection is achieved in an *in vitro* skin phantom by monitoring the impedance change of the sensor electrodes as specific binding of target proteins to antibodies on the sensor surface occurs.

## INTRODUCTION

There has been growing interest in the development and study of label-free sensors in the medical and health industry. Impedance sensors are a promising approach due to ease of miniaturization, rapid readout and label-free operation. One obstacle to adoption of label-free sensors is that they lag their fluorescent counterparts in terms of sensitivity [1]. Our previous work has demonstrated nano-well impedance sensors on glass substrates with capabilities of fM-level cytokine detection [2]. However, these sensors do not have a tissue insertion form factor. In addition, one of the primary challenges that impedes the chronic application of these sensors *in vivo* is the large mechanical mismatch between stiff material and surrounding soft tissue [3]. To address these limitations, the form factor of the sensor has been changed to a microneedle shape, and materials with lower Young's modulus (e.g., flexible polyimide or parylene materials) [4][5] have been employed in the sensor fabrication. These improvements enable a label-free impedance sensor which is flexible yet can be inserted into tissue directly. The integration of stiff insertion device to the flexible sensor could facilitate the delivery into the tissue [6].

### Methodology

The sensor, consisting of a 100  $\mu\text{m}$  x 100  $\mu\text{m}$  micro-well array comprising 169 individual wells, is configured on the tip of a flexible micromachined needle. The basic principle of this flexible impedance sensor is the continuous monitoring of the impedance change across the sensor electrodes due to specific binding of target protein to the antibody already present on the sensor. The probe

antibody of tumor necrosis factor alpha (anti-TNF- $\alpha$ ), is immobilized on the sensor surface inside the microwells. Specific binding of target protein, tumor necrosis factor alpha (TNF- $\alpha$ ), to the antibody will affect the ion transfer inside the microwells, which results in an increment of impedance between the two electrodes. As a result, real-time detection of the target protein can be achieved via continuously monitoring the impedance. In order to mimic *in vivo* measurements, the sensor-bearing microneedle is inserted into a skin phantom using a temporary stiff backing that is subsequently removed to minimize mechanical damage to tissues.

Figure 1 shows a schematic of the flexible sensor, comprising a pair of gold electrodes, separated by a 40 nm insulation layer of aluminum oxide. The mechanical and electrochemical properties of the sensor were investigated during cytokine detection. To measure sensor impedance, AC excitation and lock-in-amplifier detection were utilized. The real and imaginary components of the output voltage from the lock-in-amplifier were analyzed to identify the specific binding of the target protein to the antibody.

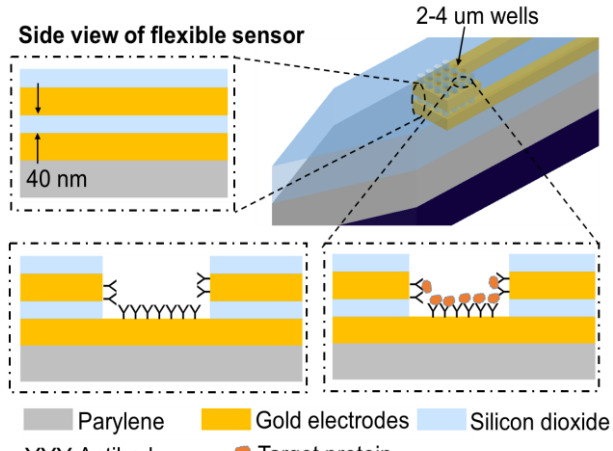


Figure 1: A schematic view of the label-free flexible sensor. Specific binding of target protein to an antibody immobilized on the sensor surface results in an increment in impedance between electrodes.

## EXPERIMENTAL

### Fabrication

Two classes of structures were fabricated in this work: microneedle sensors as well as several microfluidic skin phantoms for *in vitro* testing of the microneedle sensors. Each of these structures is described below.

The fabrication process of the microneedle sensor is schematically detailed in Figure 2. The process began by coating a bare fused silica wafer with a 7  $\mu\text{m}$  thick layer of poly-monochloro-para-xylylene (Parylene C) using an SCS PDS 2010 Parylene coater; this coating forms a base

layer of the device. A gold film (100 nm) was then deposited by e-beam evaporation on this parylene layer and patterned by lift-off, yielding the bottom layer electrode, the interconnecting line and the bonding pad. Gold was chosen as the electrode due to its inert nature and resistance to corrosion. Atomic layer deposition (ALD) was performed to deposit a 40 nm thick aluminum oxide layer as an interelectrode insulator. The top gold electrode and pad (100 nm) were patterned using the same method as for the bottom layer electrode. A 5 nm thick layer of chromium was used to enhance the adhesion of the gold film to the aluminum oxide layer. A 40 nm thick passivation layer of aluminum oxide was deposited on top of this structure by ALD. The microwells in the overlapping region of the two electrodes were patterned using sequential reactive ion etching of the aluminum oxide and wet etching of gold. Gold pads were lithographically defined and exposed for connecting and recording. The flexible sensor was laser micromachined into its needle shape using an excimer laser (IPG IX-255 excimer laser micromaching system) and released from the substrate after the immersion in DI water. To assist the insertion process, the sensor was integrated with a stainless steel insertion device of approximately 25  $\mu\text{m}$  in thickness. The insertion device was cut to the shape of the sensor using laser micromachining (IPG IX280-DXF Green Laser machining system), and integrated with the sensor using water-soluble adhesive. The use of this soluble adhesive enabled subsequent removal of the insertion device while allowing the microneedle sensor to remain embedded.

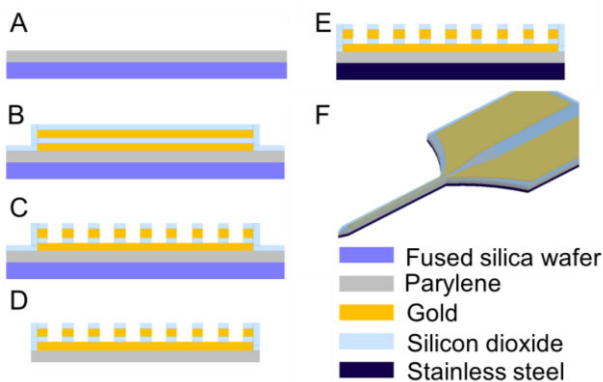


Figure 2: Process for fabricating the flexible sensor. A-E) Cross-sectional views of the micro-sized wells on sensor tip. F) A schematic 3-D view of the fabricated sensor.

The skin phantom fabrication process includes the fabrication of a phantom epidermis layer as well as the fabrication of a layer that mimics the dermis and hypodermis; this latter layer includes a microfluidic channel or well acting as a blood vessel. Both a vertical insertion phantom, in which the sensor is inserted vertically (with epidermis and lateral microfluidic channel as described in Figure 5) and a lateral insertion phantom (with larger vertical fluidic well and sidewall sensor insertion site but lacking epidermis) were fabricated. Epidermis mimicking film with thickness of 0.1 mm was prepared by spin coating PDMS (10:1 pre-polymer/ curing agent) onto a bare fused silica wafer, curing at 80 °C for 2 hours, and peeling from the wafer. To mimic the dermis

and hypodermis, a mixture of 8% gelatin (Gelatin from porcine skin, G1890 powder, Sigma-Aldrich) and 1% agar (A1296 powder, Sigma-Aldrich) was utilized. The gelatin and agar powders were dissolved in DI water using separate beakers, and each beaker was heated to 100 °C. Equal amounts of liquid from each beaker were then combined and cooled to 40 °C under constant stirring. To prepare the blood vessel mimic, this solution was added to a shallow container into which a polyetheretherketone (PEEK) tubing (outer diameter of 3 mm) had been introduced previously; a total solution height of 20 mm was used to completely submerge the tubing. The container was then held at room temperature until the solution gelled, the PEEK tubing was mechanically removed, and the epidermis-mimicking film was placed above the dermis and hypodermis-mimicking layer to form the topmost layer of the vertical insertion phantom [7]. The lateral insertion phantom was prepared in a substantially similar way by creating a disk of gelled gelatin/agar solution 11mm in diameter and 20mm in thickness; a central core 5mm in diameter and approximately 10mm in thickness was created in this disk using a punch to remove the central portion of the gelatin/agar, forming a toroidal-shaped well.

#### Electrochemical Property Characterization

Prior to any protein introduction or insertion tests, Electrochemical Impedance Spectroscopy (EIS) tests of the sensors themselves were conducted using a potentiostat (Gamry Reference 600) in a two-electrode configuration. The sensors were tested in different solution environments to investigate how the immobilization of the anti-TNF- $\alpha$  on the sensor surface inside the microwells affects ionic transport between the two electrodes. To obtain *in vitro* EIS measurements, the microwell region of the sensor was fluidically isolated using a PDMS ring into which 1X Phosphate Buffered Saline (PBS) solution was introduced. After stabilization of the resultant impedance, anti-TNF- $\alpha$  (40  $\mu\text{M}$  in 1X PBS) was added into the microwell region. During the various fluid additions, the sensor impedance as a function of time was monitored at the single frequency of 5 kHz at 20 mV excitation and at room temperature.

#### Mechanical Property Characterization

The sensor base layer was comprised of Parylene C, a Class VI biocompatible polymer that can be processed with standard micromachining technologies [5]. The low modulus of Parylene C mitigates mechanical mismatch issues between the needle-shaped sensor and the soft surrounding tissue. However, sufficient mechanical stiffness for tissue insertion (e.g., transdermal insertion) is a key design requirement. In order to assist the insertion of the sensor into the blood vessel for potential *in vivo* applications, a removable stainless steel stiff backing was utilized to facilitate the delivery of the flexible needle. Insertion experiments were carried out in the fabricated vertical insertion phantom.

#### Protein Detection

The basic principle for microwell sensor protein detection is alteration of the intrawell ionic impedance when specific binding between anti-TNF- $\alpha$  and TNF- $\alpha$  occurs inside the microwells. As described above, a lock-in-amplifier (HF2IS Impedance Spectroscope) is utilized to achieve continuous monitoring of the current through the electrodes (and therefore the electrode

impedance) in real-time.

The measurements were performed at 1 MHz at room temperature with an AC voltage of 400 mV, and using the lateral fluidic cell skin phantom to facilitate the introduction of various protein solutions. Sensors were isolated from external electromagnetic interference using a Faraday cage, significantly reducing external interference and allowing for reliable measurements at 1 MHz. After the insertion of the needle through the lateral skin phantom into the fluidic cell, 1X PBS was added to emulate the physiological environment. Then, 5  $\mu$ L of anti-TNF- $\alpha$  (40  $\mu$ M in 1X PBS) was introduced into the fluidic cell, allowing antibody absorption on the electrode surface inside the microwells. After the absorption process of the anti-TNF- $\alpha$  was completed, 15  $\mu$ L of 1X PBS was added into the fluidic cell as a negative control step. The purpose of this step is to eliminate the possible effects from 1X PBS in the following measurements due to the fact that all anti-TNF- $\alpha$  and TNF- $\alpha$  were diluted using 1X PBS. After stabilization, 5  $\mu$ L of the target protein, TNF- $\alpha$  (1 nM in 1X PBS) was added to the fluidic cell. For each step, complete stabilization of the impedance across the electrodes took less than 30 min.

## RESULTS AND DISCUSSION

### Microscopic Images

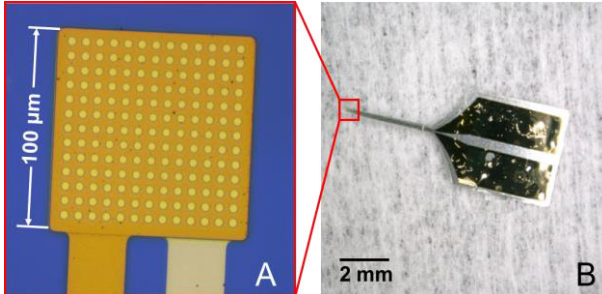


Figure 3: Microscopic images of fabricated flexible sensors. A) Sensor before detaching from wafer. B) Sensor after the alignment with stainless steel insertion device.

Figure 3 shows a functional flexible impedance sensor fabricated in a microneedle form factor. Figure 3B shows the overview of the sensor after being laser micromachined into a needle shape and integrated with the removable stainless steel insertion device; the sensor has overall dimensions of 4.5 mm x 10.5 mm. Figure 3A includes a zoomed-in micrograph of the overlapping region of two gold electrodes (100  $\mu$ m x 100  $\mu$ m) to visualize the sensing microwells.

Figure 4 shows the impedance changes across sensor electrodes after applying 1X PBS and anti-TNF- $\alpha$  on the sensor respectively. As expected, initial addition of 1X PBS resulted in significantly reduced electrode impedance (Figure 4A). After applying anti-TNF- $\alpha$  on the sensor, physical immobilization of the antibody on the surface of the electrode occurred over a time span of several minutes. The observed increase in impedance is consistent with the presence of antibody on bottom layer electrode reducing ion transfer in sensor wells, resulting in an increment in impedance (Figure 4B).

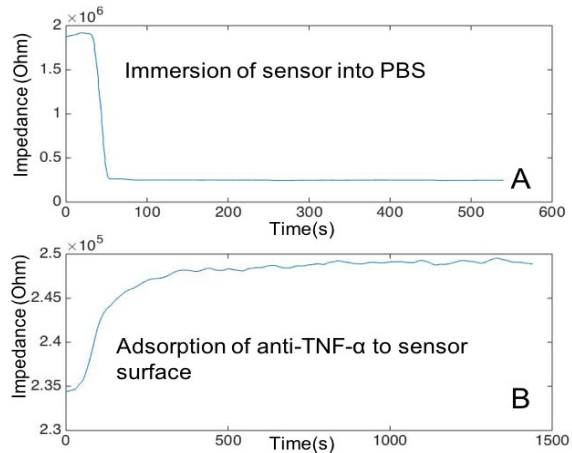


Figure 4: Impedance across sensor electrodes at 5 kHz measured by potentiostat in different sensor environments. A) Initial wetting of the sensor by adding 1X PBS to the fluidic cell resulted in a significant decrease in impedance. B) As antibodies were physically absorbed, the sensor responded with an increase in impedance.

### Mechanical Properties

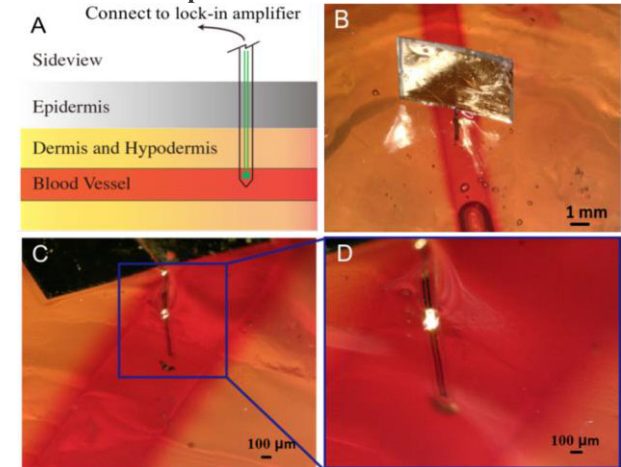


Figure 5: A) Configuration of the vertical skin phantom consisting of epidermis (PDMS), dermis and hypodermis (a mixture of gelatin and agar) and blood vessel (fluidic channel with dyed 1X PBS solution). B) Assisted by the stainless steel insertion device, the flexible sensor was inserted through the skin phantom into the fluidic channel. C), D) The stiff backing was completely removed, leaving the flexible sensor intact in the skin phantom.

The integrated needle was tested on the vertical skin phantom to determine if the proposed insertion system could effectively and reproducibly deliver flexible sensors to a desired location. The skin phantom was constructed as described above to emulate the skin tissue and a blood vessel (Figure 5A). Although parylene-based needles were relatively flexible (as designed), integration with the stainless steel backing significantly increased the stiffness during insertion. The full shank of the flexible needle was inserted through a skin phantom into a fluidic channel with the assistance of the stiff backing; no buckling occurred during sensor insertion (Figure 5B). After the insertion into skin phantom, the water soluble adhesive along the shank of the parylene-based needle dissolved, which enabled the removal of the stiff backing (Figure 5C, 5D),

demonstrating that the flexible needle was successfully delivered into the fluidic channel. The similarities in the mechanical properties between the sensor and the tissue may be useful in subsequent *in vivo* tests.

Figure 6 shows a set of representative experimental results of the immobilization of the probe antibody (anti-TNF- $\alpha$ ) on the sensor (negative control), as well as the detection of target protein (TNF- $\alpha$ ), respectively, after the insertion of the flexible sensor through the lateral skin phantom. The results show the change in output voltage, which is proportional to the current through the electrodes measured by the lock-in amplifier (and therefore inversely proportional to the electrode impedance), as a function of time. After the introduction of the anti-TNF- $\alpha$  solution onto the sensor, these antibodies were absorbed on the electrode surface, which resulted in a drop in the current through the electrodes (Figure 6A). This result also matched the increase in impedance that was measured in the fluidic cell as shown in Figure 4B. For the negative control step, when 1X PBS containing no protein was added into the fluidic cell, aside from the initial baseline shift common to all steps, the current through the electrodes generally increased by 2% (Figure 6B). This is seen with all negative control experiments, likely due to antibody desorption. After the negative control step, the current through the electrodes began to decrease as the target protein was introduced. The potential explanation for this behavior is that when specific binding of TNF- $\alpha$  to anti-TNF- $\alpha$  occurred on the electrode surface, ion transfer was reduced, which resulted in a drop of the baseline. This demonstrated the capability of the flexible sensor to detect TNF- $\alpha$  in 1X PBS at a concentration of 1 nM.

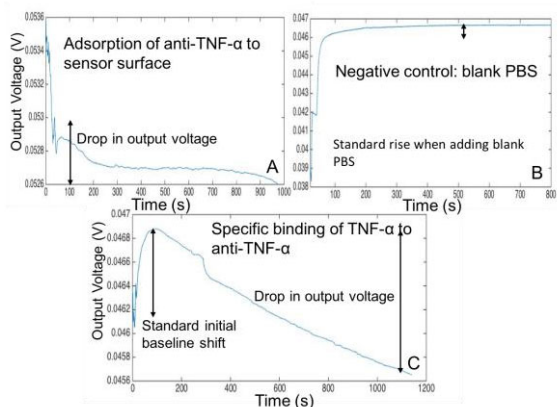


Figure 6: Lock-in amplification data at 1 MHz. Note that the y-axis of these plots, a measurement of the current through the sensor, is inversely proportional to impedance. A) After the insertion of flexible sensor through skin phantom into fluidic cell, there was a drop in current through the electrodes. B) When blank PBS was added to the fluidic cell as a negative control, the baseline generally increased. C) Specific binding of TNF- $\alpha$  to anti-TNF- $\alpha$  resulted in a drop in current after the initial baseline shift.

## CONCLUSION

In this study, we present a flexible micromachined needle-shaped impedance sensor for label-free *in-situ* detection of cytokines and other biomarkers at nM concentrations. Robust mechanical stiffness of the integrated needle and stable protein detection ability after

insertion into a skin phantom were demonstrated, which suggested the potential application to *in vivo* detection. In addition, this integration approach of flexible sensor with small stiff insertion device, followed by the removal of the insertion device, may yield benefits in chronic application of the flexible sensors. We also repeatedly validated the functionality of the flexible sensor by continuously recording in various solutions after the insertion through the skin phantom, showing that the sensors are capable of monitoring cytokines at low concentrations.

## ACKNOWLEDGEMENT

The authors acknowledge support from the DARPA Cooperative Agreement HR0011-16-2-0026 under the ElectRX program managed by Dr. Douglas Weber. Fabrication was conducted at the Singh Center for Nanotechnology at the University of Pennsylvania, which is supported by the National Science Foundation NNCI Program, #15-42153. Protein detection experiments were carried out at Rutgers University.

## REFERENCES

- [1] J. Daniels, N. Pourmand, "Label-Free Impedance Biosensors: Opportunities and Challenges", *Electroanalysis*, vol. 19, no. 12, pp. 1239-1257, 2007.
- [2] P. Xie, N. Song, W. Shen, M.G. Allen, M. Javanmard, "Nanowell Array Impedance Sensor for Label-free Quantification of Cytokines in Serum at FemtoMolar Level Detection Limits", *Miniaturized Systems for Chemistry and Life Sciences*, Savannah, GA, USA, Oct 22-26, 2017.
- [3] W. Shen, L. Karumbaiah, X. Liu, T. Saxena, S. Chen, R. Patkar, R. Bellamkonda and M. Allen, "Extracellular matrix-based intracortical microelectrodes: Toward a microfabricated neural interface based on natural materials", *Microsystems & Nanoengineering*, vol. 1, p. 15010, 2015.
- [4] K. Lee, A. Singh, J. He, S. Massia, B. Kim and G. Raupp, "Polyimide based neural implants with stiffness improvement", *Sensors and Actuators B: Chemical*, vol. 102, no. 1, pp. 67-72, 2004.
- [5] J. Kuo, B.J. Kim, S.A. Hara, C. Lee, C.A. Gutierrez, T. Hoang, E. Meng, "Fabrication of 3D parylene sheath probes for reliable neuroprosthetic recordings", *Solid-State Sensors, Actuators, and Microsystems Workshop*, Hilton Head Island, SC, USA, Jun 3-7, 2012, pp. 30-33.
- [6] D.P. O'Brien, T.R. Nichols, M.G. Allen, "Flexible microelectrode arrays with integrated insertion devices", *The 14th IEEE International Conference on Micro Electro Mechanical Systems (MEMS 2001)*, Interlaken, Switzerland, Jan21-25, 2001, pp. 216-219.
- [7] A. Chen, M. Balter, M. Chen, D. Gross, S. Alam, T. Maguire and M. Yarmush, "Multilayered tissue mimicking skin and vessel phantoms with tunable mechanical, optical, and acoustic properties", *Medical Physics*, vol. 43, no. 61, pp. 3117-3131, 2016.

## CONTACT

\*M. Allen, tel: +1-215-898-2462; mallen@upenn.edu